Open access • Proceedings Article • DOI:10.1117/12.45943

Use of rigorous vector coupled-wave theory for designing and tolerancing surface-relief diffractive components for magneto-optical heads

Charles W. Haggans, Raymond K. Kostuk

Institutions: University of Arizona

Published on: 01 Jul 1991

Use of Rigorous Vector Coupled-Wave Theory for Designing and Tolerancing Surface-Relief Diffractive Components for Magneto-Optical Heads

Charles W. Haggans and Raymond K. Kostuk

Optical Sciences Center
University of Arizona
Tucson, Arizona 85721

ABSTRACT

A rigorous coupled-wave model is presented, experimentally validated, and used for tolerancing surface-relief diffractive elements. Applications of this model in the design and tolerancing of components for magneto-optical (M-O) data storage heads are investigated.

1. INTRODUCTION

Surface-relief lithographically generated diffractive elements show promise for M-O data storage head applications due to their polarization selectivity, planar geometry, high diffraction efficiency, and manufacturability. However, previous application of surface-relief diffractive elements to M-O storage systems has been limited due to the lack of a suitable description for their polarization properties.

A model for describing these properties is presented in this paper. A general rigorous vector coupled-wave model for the calculation of the diffraction efficiency and the polarization properties of surface-relief gratings is described and validated with experimental measurements. The accuracy of the model is then analyzed. The presentation concludes with examples showing how the model can be used in the design and tolerancing of components for M-O head applications.

2. RIGOROUS COUPLED WAVE MODEL

The formalism used in this model is an extension of Moharam and Gaylord's rigorous coupled-wave analysis for volume grating diffraction.[1,2]. In this treatment, an arbitrary surface-relief profile is approximated by slicing the profile into a number of equal thickness slabs. Coupled-wave equations are then generated for the field in each slab and are solved using a state-variables method. The complex amplitudes of the reflected and transmitted diffracted orders are then generated by matching boundary conditions.

All fields are treated as vector quantities in this model. A vector approach enables the calculation of the polariation properties of diffracted beams when cross-coupling between the polarization states takes place. This condition exists when the grating vector is not in the plane of incidence. Polarization cross-coupling is a vector effect that cannot be treated using scalar approaches. Vector analysis also allows for the treatment of arbitrary incident and output polarizations.

The state of incident elliptical polarization is specified by the s and p amplitude ratio angle (α) (defined in Figure 1) and the s and p phase difference (δ). In this figure, a and b are the major and minor axis lengths for the vibrational ellipse of the incident electric vector. a_1 and a_2 are the maximum field strengths in the p and s directions, and ψ is the angle of rotation of the major axis of the ellipse from the

p axis. An additional angle (χ) is used to represent the angular ratio of the major to minor axes of the ellipse. These parameters are related by the trigonometric relations[3]:

$$\cos|\delta| = \frac{\tan 2|\psi|}{\tan 2|\alpha|} \qquad \sin|\delta| = \frac{ab}{a_1 b_1} \qquad (1)-(2)$$

$$\sin|\delta| = \frac{\sin 2|\chi|}{\sin 2|\alpha|} \qquad \tan|\alpha| = \frac{a_2}{a_1} \qquad (3)-(4)$$

$$\tan|\chi| = \frac{b}{a}. \qquad (5)$$

The output polarization parameters determined by the model are the s and p amplitude ratio angle (α) and the s and p phase difference angle (δ) for all reflected and transmitted orders. From these two parameters, the rotation angle of the polarization ellipse (ψ) can be calculated. In the conical diffraction case, the s and p directions are different for each diffracted order. These directions are defined with respect to the plane containing the propagation vector for that order and the grating vector.

The model is implemented in MATLAB, an interpreted matrix manipulation language. Runs are currently made on a 33MHz/386 personal computer and a VAX 8650. Typical run times are 3 seconds per data point for a single step grating (nt=1 and ns=9) and 5 minutes per data point for a ten step grating (nt=10 and ns=9).

3. EXPERIMENTAL VALIDATION OF THE MODEL

Model predictions were compared to experimental measurements made in our laboratory and to the published results of two other research groups. The diffraction efficiency and polarization properties of a trapezoidal profile photoresist grating were measured in our laboratory. This grating was fabricated holographically in Shipley 1811 photoresist. The substrate was a microscope slide. Measurements were made in reflection with an absorbing layer index-matched to the back surface of the substrate to eliminate Fresnel reflections from that surface. The incident beam was linearly polarized at a 45° angle to the s and p axes. The experimental reflected diffraction efficiency (η) was defined as the measured power diffracted into the +1st reflected order divided by the measured incident power.

The polarization rotation angles ψ and χ were measured by both a direct and an indirect method. In the direct method, a linear polarizer was used to measure ψ. When the transmission axis of the polarizer was aligned with the major axis of the polarization ellipse, the maximum power was transmitted. For this condition, ψ was the angle between the polarizer transmission axis and the p axis.

χ was measured using a linear polarizer and a quarter-wave plate. The fast axis of the quarter-wave plate was aligned with the major axis of the ellipse. This eliminated the 90° phase difference between the linear polarization components along the b and a axes, giving linearly polarized light. The plane defined by the linear polarization was rotated an angle χ from the major axis of the ellipse. This angle was measured using a linear polarizer as described above.

In the indirect method, the magnitudes of ψ and χ were calculated from four power measurements. The measured powers were proportional to $|a_1|^2$, $|a_2|^2$, $|a|^2$, and $|b|^2$. $|a_1|^2$ and $|a_2|^2$ are proportional to the power transmitted by a linear polarizer aligned with the p and s axes. Similarly, powers proportional to $|a|^2$ and $|b|^2$ are measured for a polarizer aligned with the major and minor axes. $|\psi|$, $|\chi|$, $|\delta|$, and $|\alpha|$ were then calculated using equations (1)-(5).

These two methods for characterizing the output elliptical polarization state complement each other. The transmission axis of a single linear polarizer must be accurately aligned in the indirect power measurement method. In the direct measurements, both a linear polarizer and the fast axis of a quarter-wave plate must be accurately positioned. Thus, the indirect method give $|\psi|$ and $|\chi|$ more precisely than direct measurements. The direct measurement of ψ and χ gives the sense of rotation of the angles. This is useful because the sign of δ is the same as the sign of χ. [3]

The geometrical and physical properties of the grating were determined for input into the model. The grating period was determined optically to be .429 ± .0005 μm. This value was obtained by retroreflecting the +1st diffracted order onto the incident beam. The angle of rotation of the grating to achieve this condition (θ) gives the grating period according to:

$$\Lambda = \frac{\lambda}{2\sin\theta}. \qquad (6)$$

In this relation, Λ is the grating period and λ is the wavelength of the incident light. This value was then used to calibrate the Scanning Electron Micrograph (SEM) (Figure 2). The grating depth was estimated from this photo to be .22 ± .01 μm. A 10 step approximation to the grating profile was made by averaging the profiles of the six visible grating ridges and 11 coupled waves were retained in the analysis. The index of refraction of the substrate was measured to be 1.51 using a Brewster's angle technique, and the published Shipley photoresist index of refraction is 1.64 at .6328 μm.

Figures 3 through 5 compare the experimental and calculated values of diffraction efficiency, α, and $|\delta|$ for the +1st reflected order diffracted by this grating. To obtain the best fit to the experimental data, iterations were made over the uncertainty range of the grating depth and grating profile measurements. Figure 3 shows diffraction efficiency (η) versus angle of incidence, Figure 4 shows +1st order polarization ratio angle (α) versus angle of incidence, and Figure 5 shows the phase difference magnitude ($|\delta|$) versus angle of incidence. Good agreement was obtained for all parameters.

Our model predictions were compared to published experimental results from a study of the antireflection properties of short period gratings.[4] In this work, Enger and Case fabricated gratings etched in fused quartz substrates with periods short enough to supress all propagating diffraction orders. They observed significant phase differences between the s and p polarizations of the zeroth order transmitted beam. Figure 6 shows the best fit to their experimental measurements and our model calculations of phase difference as a function of grating depth for gratings of approximately triangular profile. The physical parameters of their grating no.8 were used as input for our model. This grating has a period of .31 μm, the refractive index of the quartz substrate is 1.46, and measurements were made at a wavelength of .6328 μm. An 8 step profile approximation was used and 9 coupled-waves were retained in the analysis. Nearly exact agreement was obtained over a 1 μm range of depths.

Finally, a comparison was made to work originally performed by Moharam, et. al.[5] and later by Nakata and Koshiba[6]. Coupled wave (C-W) and boundary-element (B-E) theory were used respectively in these studies to calculate the transmitted diffraction efficiency of high aspect ratio photoresist gratings. The diffraction efficiency of two gratings was measured for s and p polarized light by the original authors. The s and p component diffraction efficiencies for grating no.8 were calculated using our model. This grating has a period of .458 μm, a refractive index of 1.64, a depth of .59 μm, and an undercut profile.

Figure 7 shows the experimental measurements and the calculations of the three models for the diffraction efficiency of s polarized light as a function of angle of incidence. Figure 8 is the corresponding plot for p polarization. Our calculations deviated from the measured data in the manner of the previous studies for s polarization for angles of incidence between 15° and 25°. The B-E model provides the best fit to the measured data for large angles of incidence. However, our calculations

tend to agree with experiment better than the previous C-W model predictions. For p polarization, our model provided a better fit to the experimental data for large angles of incidence than either of the two previous models. However, it exhibited increased deviations from experiment from 25° to 40°.

Because the parameters input to the previous C-W model are not known, it is not possible to determine the cause of the poor agreement between the two models. The rigorous coupled-wave formalism used in our model reduces to the scalar coupled-wave formalism used in the previous C-W model. Thus, we assume that differences in the predictions of the two models occur because of differences in the approximation of the grating profile.

4. ACCURACY OF MODEL PREDICTIONS

Three factors determine the accuracy of the model in predicting experimental measurements: The accuracy of measurement of the physical properties of the grating, the precision with which the grating profile is approximated, and the numerical precision of the model.

For exact reproduction of the experimental measurements, the grating profile must be exactly characterized. Some physical parameters such as the grating period, the angle of incidence, and the refractive indices can be accurately determined. However, the grating depth and the grating profile are difficult to characterize. Measurement of these two parameters is limited by the irregularity of the grating ridges and by lack of contrast of the SEM photograph.

The precision of the approximation of the grating profile is determined by the number of slabs (nt) used in the approximation. The numerical precision of the model is determined by the number of coupled waves (ns) retained in the analysis. For perfect grating characterization, each output parameter converges to a constant value as nt and ns are increased.

The effects of inaccurate profile determination and insufficient numerical precision are readily observable from Figures 9 and 10. Figure 9 shows the calculated reflected +1st order diffraction efficiency versus ns for 5, 8, 10, and 12 approximations to the profile of Figure 2 for an incidence angle of 35°. Figure 10 is a similar plot for the reflected s and p phase difference. In these figures, the curves for nt=8 and nt=12 converge to efficiency values that are larger than those for the nt=5 and nt=10 curves. If the shapes of the curves changed as nt increased, the precision of the approximation of the profile would be in question. For this situation, increasing nt would cause a convergence in profile shape. However, the similar shape of the curves indicates that error in duty cycle measurement is responsible for the different efficiencies at convergence. This source of error limits the accuracy of the comparison to experiment to approximately 5 degrees for the phase difference angle and .5% for the diffraction efficiency for the grating of Figure 2.

The convergence of the curves in Figures 9 and 10 indicates that the numerical precision of the predictions increases as ns increases. The phase difference curves of Figure 10 can be observed to converge slower than the diffraction efficiency curves of Figure 9. This indicates that diffraction efficiency is less sensitive to the numerical precision of the model. Thus, the phase difference is a better indicator of the level of model precision.

These figures show that the precision of the profile approximation and the numerical precision of the model are satisfactory for this grating for coarse profile approximations and a small number of retained orders. This is evident from the similarity of the curve shapes and the rapid convergence of each curve. Sufficient precision for small values of ns and nt is computationally advantageous because the execution time of the model increases rapidly as these parameters increase.

5. APPLICATION TO MANUFACTURING TOLERANCE ANALYSIS

This model demonstrates that small errors in the fabrication of surface-relief gratings (depth, period, etc.) can cause substantial deviations from designed performance. These deviations are especially important as the grating period decreases and for high aspect ratio gratings.

The impact of manufacturing errors can be quantified by the comparison of calculated diffraction efficiencies over a hypothetical range of grating parameter values. Figure 11 shows theoretical first order diffraction efficiency curves for a two step approximation to a trapezoidal grating for three closely spaced grating periods (1.0, 1.1, and 1.2 μm). This figure shows that a .2 μm change in the grating period can cause as much as a 30% change in the diffraction efficiency. Since an optimistic tolerance in the fabrication of grating structures using lithographic techniques is of this order, it can be seen that manufacturing tolerances limit the performance of high spatial frequency lithographically generated gratings.

6. APPLICATION TO POLARIZING ELEMENT DESIGN

A unique aspect of this model is its three-dimensional efficiency surface generation module. This module can be used as an aid in designing complex elements. The output of this module is a three-dimensional plot of diffraction efficiency versus two grating parameters (i.e., grating period and grating depth, duty cycle and wavelength, etc.). Using this module, design points can be generated from a wide range of input parameters in a single run.

An example of the utility of this module is the design of rectangular profile polarization selective and nonselective elements. Figure 12 shows the diffraction efficiency for the 1st transmitted order as a function of grating depth and period for s and p polarizations for a square profile grating. Note that point B exhibits high s and low p efficiency, giving a design point for a polarization selective element for leaky beamsplitting applications. Figure 13 is the indicated cross-section of this surface in the .45 μm grating period plane. Alternatively, point A shows high s and p diffraction efficiency into the 1st transmitted order, forming a polarization nonselective element. Figure 14 shows the indicated cross-section in the .6 μm grating period plane.

7. CONCLUSION

A model for calculating the diffraction efficiency and polarization properties of surface-relief diffractive structures has been presented. Three examples of the validity of this model's predictions have been given. Use of the model for tolerancing and design of diffractive components has been presented.

8. ACKNOWLEDGEMENTS

This research was supported by an IBM University grant SUR-0449 and the Optical Data Storage Center at the University of Arizona.

The authors also wish to thank Lifeng Li and Keith Bates of the Optical Data Storage Center for supplying the photoresist grating for our experimental measurements. The authors gratefully acknowledge numerous helpful discussions with Lifeng Li and Kevin Erwin, also of the Optical Data Storage Center, and with Teruo Fujita of the Consumer Electronics Development Laboratory, Mitsubishi Electric Corporation.

9. REFERENCES

1. M.G. Moharam and T.K. Gaylord, "Three Dimensional Coupled Wave Analysis of Planar-Grating Diffraction," J. Opt. Soc. Am., Vol. 73, 1105-1112 (1983).

2. M.G. Moharam and T.K. Gaylord, "Diffraction Analysis of Dielectric Surface Relief Gratings," J. Opt. Soc. Am., Vol. 72, 1385-1392 (1982).

3. M. Born and E. Wolf, Principles of Optics, 6th ed., Pergamon Press, Oxford, 1980.

4. R.C. Enger and S.K. Case, "Optical Elements With Ultrahigh Spatial Frequency Surface Corrugations," Appl. Opt., Vol. 22, 3220-3228 (1983).

5. M.G. Moharam, T.K. Gaylord, G.T. Sincerbox, H. Werlich, and B.Yung, "Diffraction Characteristics of Photoresist Surface-Relief Gratings," Appl. Opt., Vol. 23, 3214-3220 (1984).

6. Y. Nakata and M. Koshiba, "Boundary-Element Analysis of Plane-Wave Diffraction from Groove-Type Dielectric and Metallic Gratings," J. Opt. Soc. Am., Vol. 7, 1494-1502 (1990).

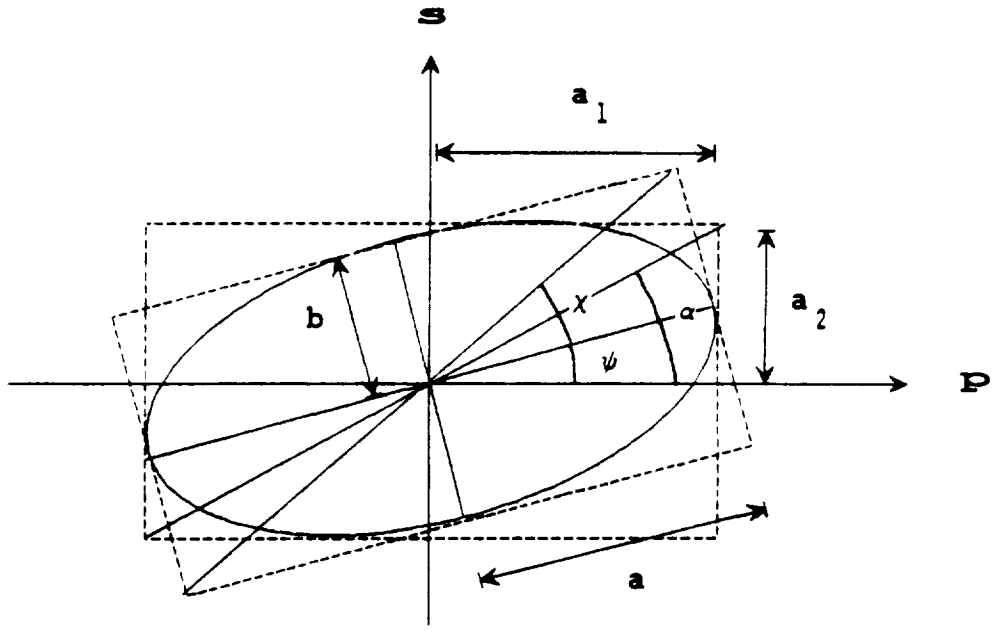

Fig. 1. Vibrational ellipse of the electric field for elliptical polarization.

Fig. 2. Scanning electron micrograph of the photoresist grating measured in our laboratory.

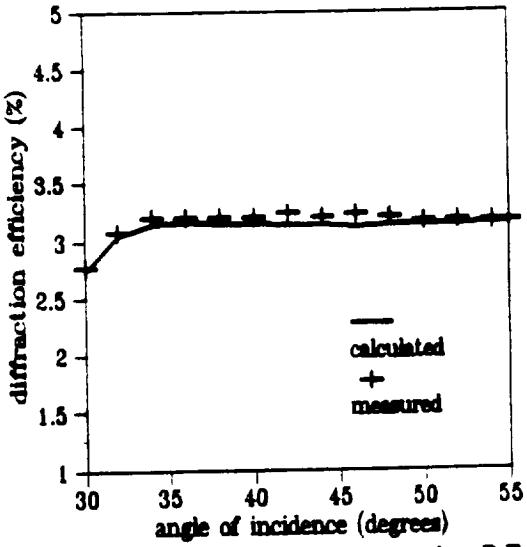

Fig. 3. +1st reflected order D.E. for the grating in Fig. 2.

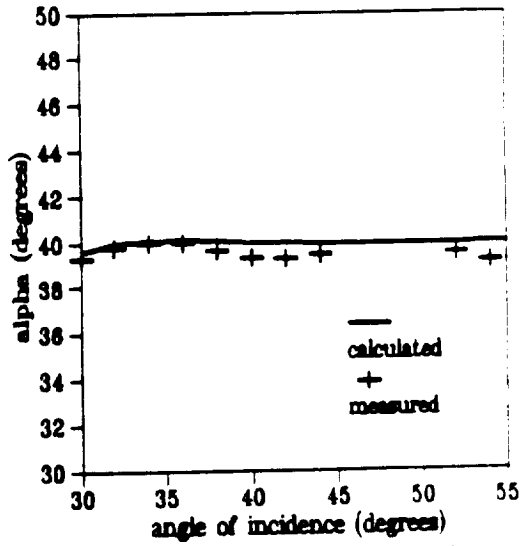

Fig. 4. +1st order polarization ratio angle for the grating in Fig. 2.

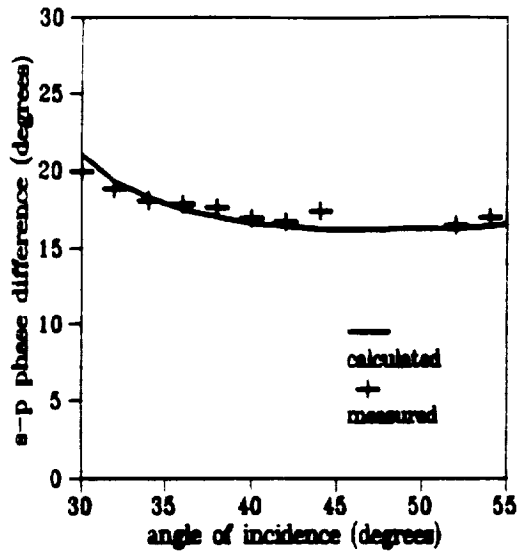

Fig. 5. +1st reflected order s-p phase difference for the grating in Fig. 2.

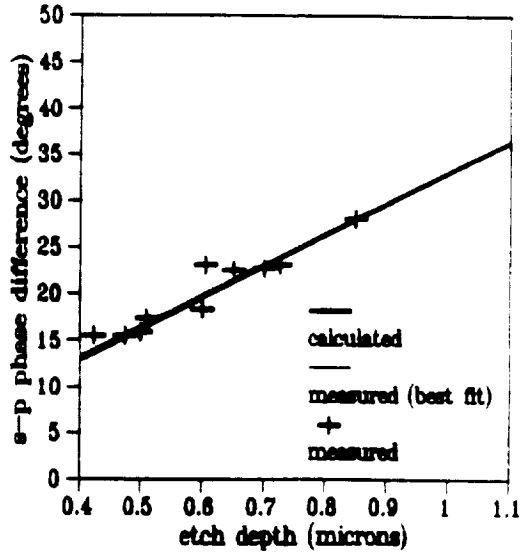

Fig. 6. Phase difference vs. etch depth for grating 8 from reference 4.

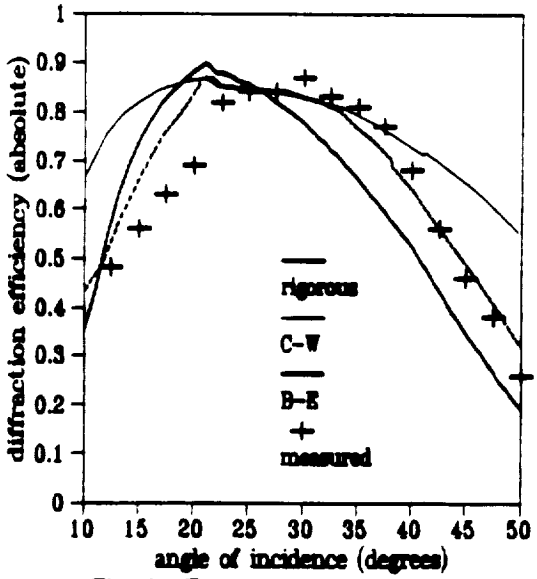

Fig. 7. Transmitted D.E. of grating 8 of reference 6 for s polarization.

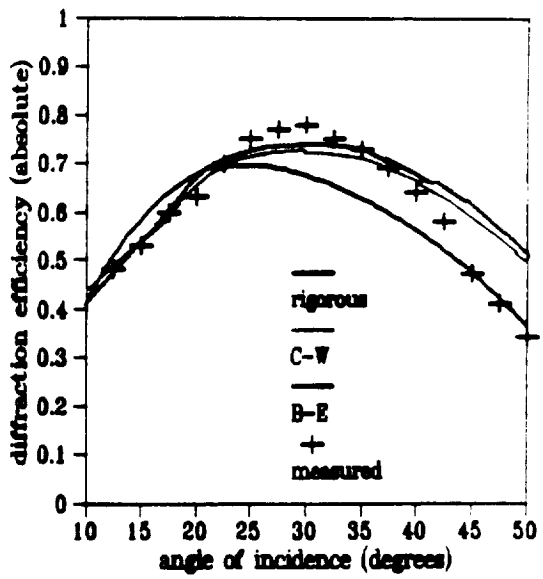

Fig.8. Transmitted D.E. of grating 8 of reference 6 for p polarization.

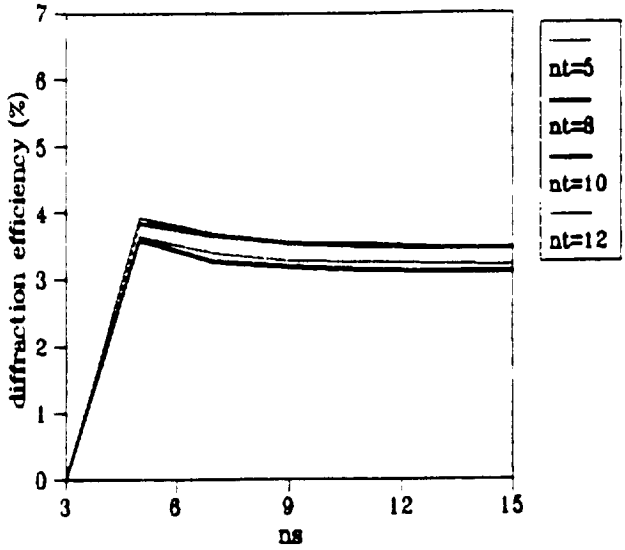

Fig. 9. Reflected +1st order DE vs. ns calculated for the grating in Figure 2.

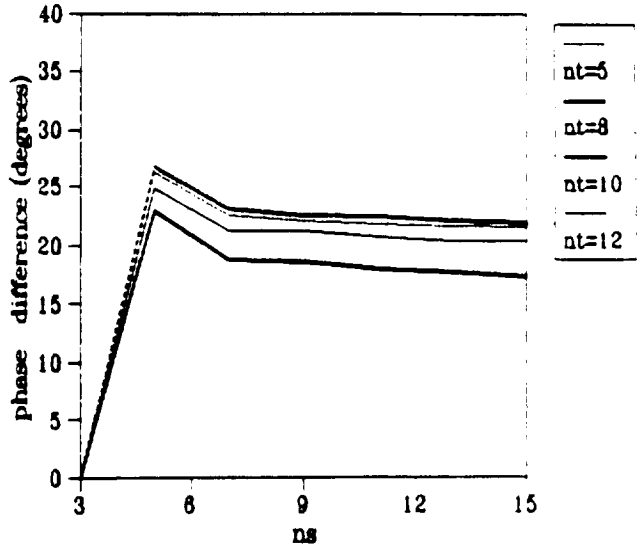

Fig. 10. Reflected phase difference vs. ns calculated for the grating in Fig.2.

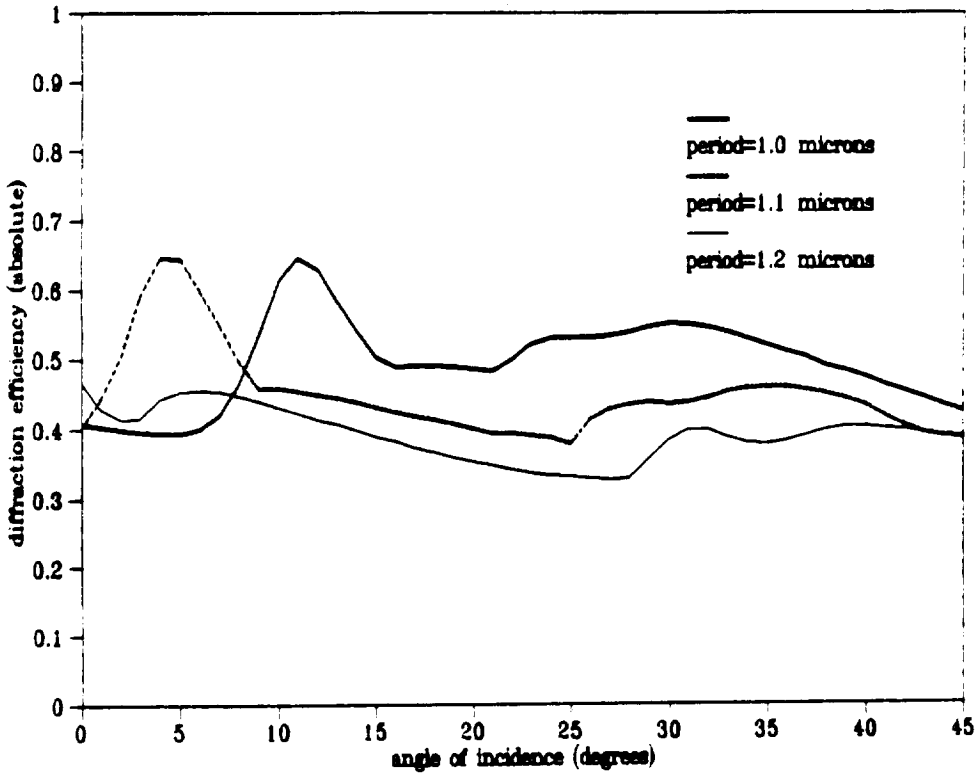

Fig. 11. +1st transmitted order diffraction efficiency for s polarization vs. angle of incidence for a two slab photoresist grating (n=1.64) of .55 micron depth on a glass substrate (n=1.51) at a wavelength of .6328 microns. The duty cycles of the two slabs are 23.8% and 38.1% respectively, and the first slab is positioned on the second slab to give even symmetry in the grating profile.

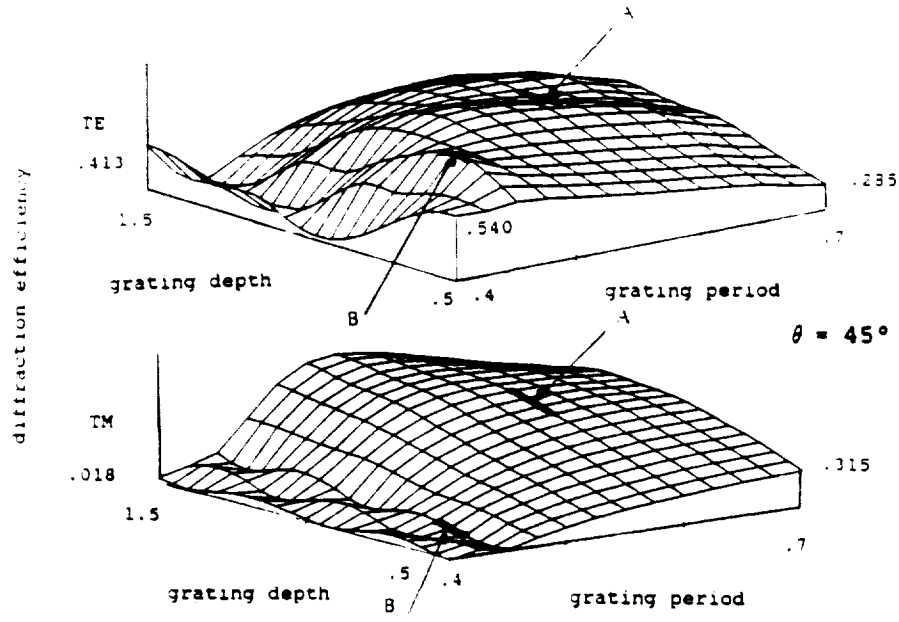

Fig. 12. +1st transmitted order diffraction efficiency for s and p polarizations vs. grating depth and period for a rectangular profile photoresist grating (n=1.68) at a wavelength of .780 microns. The duty cycle of the grating is 60%.

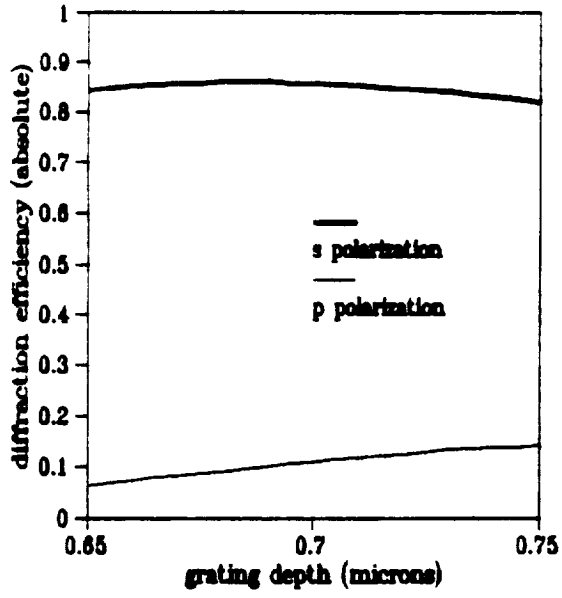

Fig. 13. Cross-sectional profile B of Fig.12 for grating period=.45 microns.

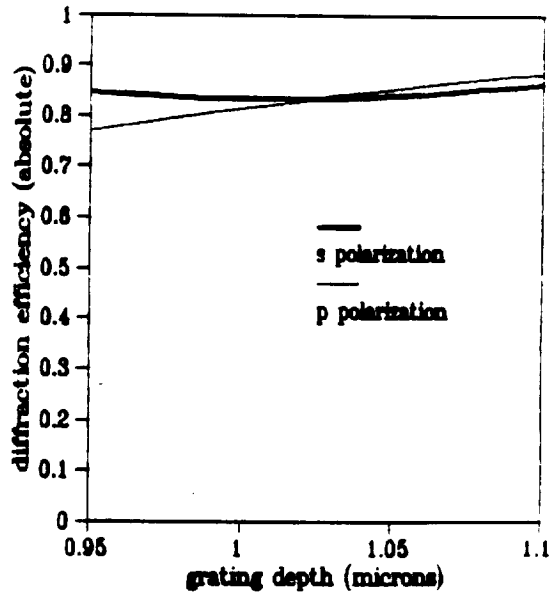

Fig. 14. Cross-sectional profile A of Fig.12 for grating period=.6 microns.